ADVANCING EARTH AND SPACE SCIENCES

Geophysical Research Letters

RESEARCH LETTER
10.1029/2025GL120494

Crustal Heat Flow Drives the Earthquake Magnitude Distribution

P. Corrado[1], **M. Taroni**[2], **L. Cordrie**[3], **R. Basili**[2], **W. Marzocchi**[1,4], **and J. Selva**[1,5]

[1]Dipartimento di Scienze della Terra, dell'Ambiente e delle Risorse, Università degli Studi di Napoli Federico II, Napoli, Italy, [2]Istituto Nazionale di Geofisica e Vulcanologia, Roma, Italy, [3]CINECA, Bologna, Italy, [4]Scuola Superiore Meridionale, Naples, Italy, [5]Istituto Nazionale di Geofisica e Vulcanologia - Osservatorio Vesuviano, Napoli, Italy

Key Points:

- The *b*-value increases with the increase of the heat flow
- The correlation between *b*-value and heat flow is generally consistent across tectonic environments and the fault kinematics

Supporting Information:

Supporting Information may be found in the online version of this article.

Correspondence to:

P. Corrado,
paola.corrado@unina.it

Citation:

Corrado, P., Taroni, M., Cordrie, L., Basili, R., Marzocchi, W., & Selva, J. (2026). Crustal heat flow drives the earthquake magnitude distribution. *Geophysical Research Letters*, *53*, e2025GL120494. https://doi.org/10.1029/2025GL120494

Received 6 NOV 2025
Accepted 12 FEB 2026

Author Contributions:

Conceptualization: P. Corrado, M. Taroni, R. Basili, J. Selva
Data curation: M. Taroni, R. Basili
Formal analysis: P. Corrado
Funding acquisition: J. Selva
Investigation: P. Corrado, M. Taroni, L. Cordrie, R. Basili, W. Marzocchi, J. Selva
Methodology: P. Corrado, M. Taroni
Project administration: J. Selva
Software: P. Corrado
Supervision: M. Taroni, R. Basili, J. Selva
Validation: P. Corrado, M. Taroni, W. Marzocchi, J. Selva
Visualization: L. Cordrie
Writing – original draft: P. Corrado
Writing – review & editing: P. Corrado, M. Taroni, L. Cordrie, R. Basili, W. Marzocchi, J. Selva

Abstract Earthquake magnitude-frequency distributions exhibit significant space-time variations, which can provide critical insights into the physical processes driving seismicity. Understanding these variations is crucial for assessing seismic hazards and uncovering the physical processes driving earthquakes. One key parameter, the *b*-value, describes the relative proportion of small to large earthquakes and is thought to reflect factors such as stress conditions and fault properties. However, empirical evidence linking *b*-value variations to physical processes in real tectonic settings is still limited. Here, we show that *b*-value is systematically higher in regions with elevated heat flow, consistently across different tectonic settings and faulting style. This suggests that thermal conditions play a fundamental role in controlling earthquake size distributions, controlling the likelihood of large earthquakes in the different areas.

Plain Language Summary Earthquakes come in many sizes, from small ones that often go unnoticed to large, damaging ones. The magnitude-frequency distribution (MFD) is a tool that is frequently used to understand how often earthquakes of different sizes happen. A key part of this tool is the *b*-value, which tells us how many small earthquakes occur compared to large ones. This study explores what controls the *b*-value around the world. Specifically, it investigates whether the amount of heat flowing from the Earth's interior—known as heat flow—affects how often large earthquakes occur. By analyzing more than 22,000 earthquakes from a global catalog, we found that regions with higher heat flow tend to have higher *b*-values. This means that in hotter areas of the Earth's crust, small earthquakes are relatively more common and large ones less likely. The study shows that this relationship between heat flow and *b*-value holds true regardless of tectonic setting or type of fault movement. These findings suggest that temperature plays a major role in shaping earthquake behavior.

1. Introduction

Space-time variations observed in the earthquake magnitude-frequency distribution (magnitude-frequency distributions [MFD]) are particularly intriguing as they could provide important physical insights into the processes driving future earthquakes. These variations are typically analyzed as spatiotemporal changes in the MFD's key parameter, the *b*-value, which represents the slope of the distribution log-linear part (Kagan, 2002).

Such changes are often interpreted as signatures of the underlying physical processes, for example, variations of differential stress (Amitrano, 2003; Goebel et al., 2013; Gulia & Wiemer, 2010; Gulia et al., 2018, 2020; Scholz, 2015; Schorlemmer et al., 2005; Tormann et al., 2015), or as features of the lithology and geometry of the faults (Aki, 1981; Collettini & Tinti, 2025; Herrmann & Marzocchi, 2021; Hirata, 1989). Most of these physical interpretations stem from analog observations made during experiments but are rarely supported by solid empirical evidence from real tectonic earthquakes. Despite the apparent simplicity of calculating the *b*-value, many space-time variations of the *b*-value may be attributed to space-time catalog incompleteness or the lack of constraints on MFD's upper bound (Corrado et al., 2025; Herrmann & Marzocchi, 2021; Kagan, 1999, 2002, 2003; Marzocchi et al., 2020).

At a global level, spatial variations in the *b*-value have been observed primarily in relation to the earthquake focal mechanism (e.g., Petruccelli et al., 2018, 2019; Schorlemmer et al., 2005), while studies on the influence of tectonic setting presented mixed results. For instance, Bird and Kagan (2004) find significant changes across different tectonic settings only in the corner magnitude, not in the *b*-value, whereas Kagan et al. (2010) identify significant deviations of the *b*-value only in spreading ridges. Here, we aim to investigate the potential physical causes of such global variations of the *b*-value, examining the statistical correlation with a measurable physical quantity, the heat flow. Heat flow emerges as a good candidate due to its influence on b-value variations in volcanic regions and crustal areas with significant thermal variations, such as California (Cheng et al., 2020; Enescu et al., 2009; Manganiello et al., 2023; Nandan et al., 2017). In particular, Cheng et al. (2020), apply a geographic-detector approach to identify spatially varying, potentially non-linear dependencies between heat flow and earthquake size distribution in tectonically active zones at the global scale. Their analysis, which is focused primarily on subduction zones and based on the ISC catalog, reveals a characteristic pattern: a negative correlation between heat flow and b-value below 84 $\mathrm{mWm^{-2}}$ and a positive correlation above this threshold. This nonlinearity suggests that thermal conditions may influence seismicity differently across distinct thermal regimes.

In this work we revisit the heat flow-b-value question using the entire Global CMT catalog, which provides homogeneous magnitudes and mechanism estimates across all tectonic settings (including spreading ridges and strike-slip faults) together with explicit, time-varying completeness estimates and estimation methods that account for variable completeness (Taroni, 2021; Taroni et al., 2021).

2. Methods

2.1. Estimation of the Completeness Magnitude (M_C)

In this work, we use Taroni's (2023) method, which applies the Lilliefors tests (Herrmann & Marzocchi, 2021), to check the magnitudes' exponentiality as implied by the Gutenberg-Richter law (Aki, 1965). The method proposed by Taroni (2023) method is particularly suitable for a catalog containing events that might have different b-values, as in the global CMT catalog. To avoid bias in the estimation, we split the catalog into two temporal windows, 1980–2003 and 2004–2023, because in 2004, there were improvements in the methods for event detection (Ekström et al., 2012). We obtain $M_C = 5.5$ in the first part and $M_C = 5.1$ in the second part. Moreover, we also consider the short-term catalog incompleteness, which is present in the global CMT catalog (Iwata, 2008; Kagan, 2004), by increasing the completeness magnitude by 1.0 in the first 24 hr after each M_W 7.0+ event (thus $M_C = 6.5$ in the first part, and $M_C = 6.1$ in the second part of the catalog). To ensure the robustness of our results, we also consider conservative thresholds for completeness by increasing all the previous values by 0.2 and selecting the events accordingly.

For confirmatory results using even a more conservative estimation of the completeness, we also increase it by 1.5 in the first 48 hr after each M_W 7.0+ event. All the results are listed in Table S1 in Supporting Information S1.

2.2. Estimation of the b-value

Once the magnitude of completeness M_C is estimated, we compute the b-value of each sub-catalog using the method proposed by Taroni (2021), which considers the variability of the M_C with time. This method consists of subtracting to each magnitude of the data set (M_i) the value of the completeness magnitude at that time ($M_C(t)$); the quantity $X_i = M_i - M_C(t)$ can be used in the classical maximum-likelihood estimation for the b-value and for its related uncertainty σ (Aki, 1965). If we consider the correction for the finiteness of the sample (n is the number of events in the data set), we obtain (Marzocchi et al., 2020):

$$\hat{b} = \frac{\frac{n-1}{n}}{\ln(10)\left(\frac{\sum_{i=1}^{n} X_i}{n}\right)} \tag{1}$$

$$\hat{\sigma}_{\hat{b}} = \frac{\hat{b}}{\sqrt{n}} \tag{2}$$

In our case, since the magnitudes of the CMT catalog are derived from the seismic moment, the magnitude binning does not introduce any significant bias in the analysis carried out in this paper.

An effective tool to remove the effects of the short-term aftershock incompleteness exists (b-positive, van der Elst, 2021), but its applicability requires that earthquake pairs share a similar level of completeness, which is only ensured when events occur within a limited spatial and temporal range. If earthquakes are too far apart, differences in network coverage and detection capabilities can lead to variable completeness magnitudes, thereby biasing the estimate (Lippiello & Petrillo, 2024). In our study, events are grouped by heat-flow bins rather than proximity, combining earthquakes that may be widely separated geographically and temporally. Under such heterogeneous conditions, applying the b-positive method violates its fundamental assumptions and could lead to unknown bias on the b-value estimates. Therefore, we adopt the joint estimation approach of Taroni et al. (2021), which explicitly accounts for spatial and temporal variations in completeness and is better suited to our data set.

For the estimation of the b-value along with the corner magnitude, that is the two parameters estimation of the tapered Gutenberg-Richter distribution, we use the method of Taroni et al. (2021).

2.3. Significance of *b*-value Differences

To determine whether there is a statistically significant difference between b-values (Figure S6 in Supporting Information S1), we use the two-sample Utsu test (Utsu, 1966), which has been commonly adopted in several b-value studies and can be applied in the case of a magnitude of completeness changing with time (Taroni, 2021). We interpret p-values within the Neyman–Pearson framework, using them only to determine whether they fall below the predefined significance threshold, without attributing intrinsic meaning to their numerical value. However, we still report the p-values because they provide an additional piece of information: from Fisher's perspective, the p-value represents how likely it would be to observe the observed data if the considered hypothesis were true.

We initially set a significance level of 0.01. Then, to account for multiple tests, we adjust the significance level to $0.01/N$, where N represents the number of tests conducted (Bonferroni, 1936), in our case $N = 4$ (Figure S6 in Supporting Information S1; results with p-values below this adjusted threshold are marked in bold, indicating significant differences).

2.4. Other Statistical Tests

To compare the heat flow distributions for events in different tectonic environments, we use the classical Mann-Whitney statistical test; to compute the correlation between the b-value and heat flow, we use the Pearson correlation coefficient; for the b-value comparison between two groups, we also use the two-sample Kolmogorov-Smirnov test (all these tests can be found in Gibbons & Chakraborti, 2003). In all these cases, we use the Bonferroni correction (Bonferroni, 1936) to account for multiple tests.

3. Data

3.1. Catalog and Heat Flow Model

In this work, we use the global CMT catalog (Dziewonski et al., 1981; Ekström et al., 2012) from 1980 to 2023, with a maximum depth of 50 km (Schorlemmer et al., 2005). We assign each event to a specific tectonic environment according to Kagan et al. (2010), who identify four main tectonic zones: plate interior, active continent, ridge, and trench. We chose to omit results from the plate interior zone due to an insufficient amount of data, which prevents reasonable statistical analyses. Using the information of the focal mechanism contained in the CMT catalog and according to Anderson's theory (Anderson, 1905) and the Aki-Richards (Aki & Richards, 2002) convention, we classify events with a rake of $[-135, -45]$ as normal, those with a rake of $[45, 135]$ as reverse, and the rest as strike-slip. We then assign the heat flow value according to the worldwide (2° equal area grid) model of Davies (2013) to each earthquake using bilinear interpolation over the four nearest values of the Davies model to each epicenter.

In addition, we implement a complementary selection procedure to ensure that only reliable heat flow information is considered. For each grid cell of the Davies model (Davies, 2013), we calculate the relative error as the ratio between the reported uncertainty and the mean heat flow value. Cells with a relative error lower than the median are retained, while those with larger uncertainties are excluded. During the assignment of heat flow values to earthquakes, we again consider the four nearest cells; if at least one of them has been excluded due to large uncertainty, the corresponding event is discarded. Otherwise, the heat flow is computed as an inverse-distance weighted average of the four selected values. All analyses are repeated following this procedure and listed in the supplementary material (Table S2 in Supporting Information S1), using only earthquakes associated with reliable heat flow estimates and removing the potential influence of poorly constrained values.

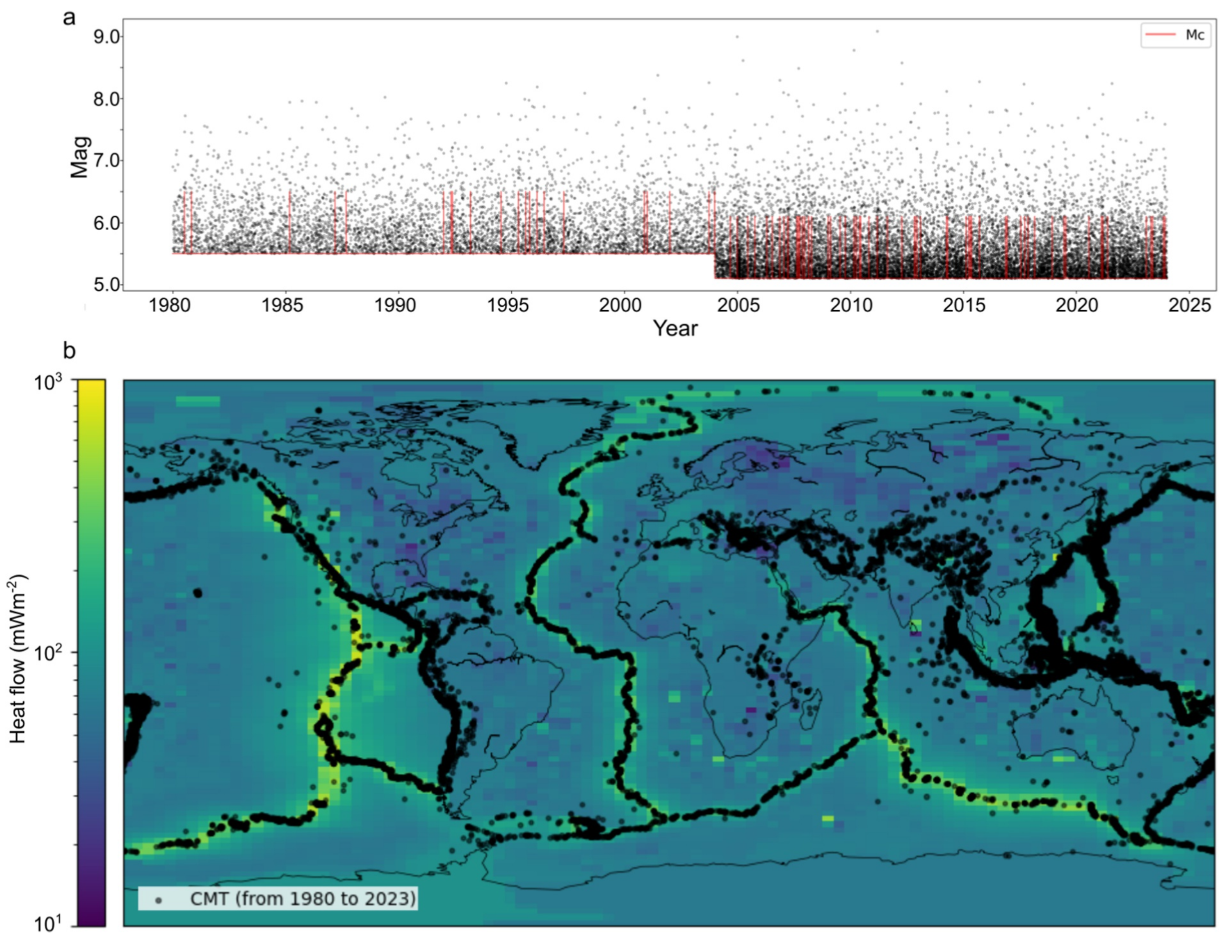

Figure 1. Temporal and spatial distribution of the events. (a) Timeline of the events of the CMT catalog above the completeness magnitude (M_C; red line); (b) Distribution of the epicenters of the CMT catalog (Dziewonski et al., 1981; Ekström et al., 2012) of the events with a magnitude above the M_C overlain onto the heat flow model (Davies, 2013). For comparison with a more conservative M_C see Figure S1 in Supporting Information S1.

4. Results and Discussions

We consider the events provided by the Global CMT (Dziewonski et al., 1981; Ekström et al., 2012), which represents one of the most homogeneous existing seismic catalogs. We pay special attention to the completeness of the earthquake catalog, as data incompleteness can significantly bias the estimation of the *b*-value. To address this issue and ensure unbiased estimation of MFD parameters, we calculate the completeness magnitude through time with different methods (see Methods), accounting for both changes in detection systems (Ekström et al., 2012; González, 2024) and potential short-term variations (Iwata, 2008).

The procedure yields a time-varying completeness magnitude (Figure 1a) and leads to a complete and homogeneous worldwide catalog from 1980 to 2023. Limiting to a maximum depth of 50 km (Petruccelli et al., 2019; Schorlemmer et al., 2005), the catalog contains a total of 22,475 seismic events (Figure 1b).

To introduce the heat flow variable in our computation, we quantify the local heat flow in the epicentral area of each event in the CMT catalog using the global heat model from Davies (2013) (see Methods for details and Figure 1b). The MFD is then quantified by grouping the events with similar heat flow, independently from their location, and then estimating the Gutenberg-Richter *b*-value (see Methods). We identify a significant global correlation between the *b*-value and heat flow (Figure 2a), with higher *b*-values for higher heat flows.

Since the heat flow distributions in the different tectonic environments (Bird, 2003) are significantly different from each other (see Section 2, Table S3 and Figure S5 in Supporting Information S1), this result would provide a potential physical explanation for the observations that *b*-values are significantly different in the different tectonic

10.1029/2025GL120494

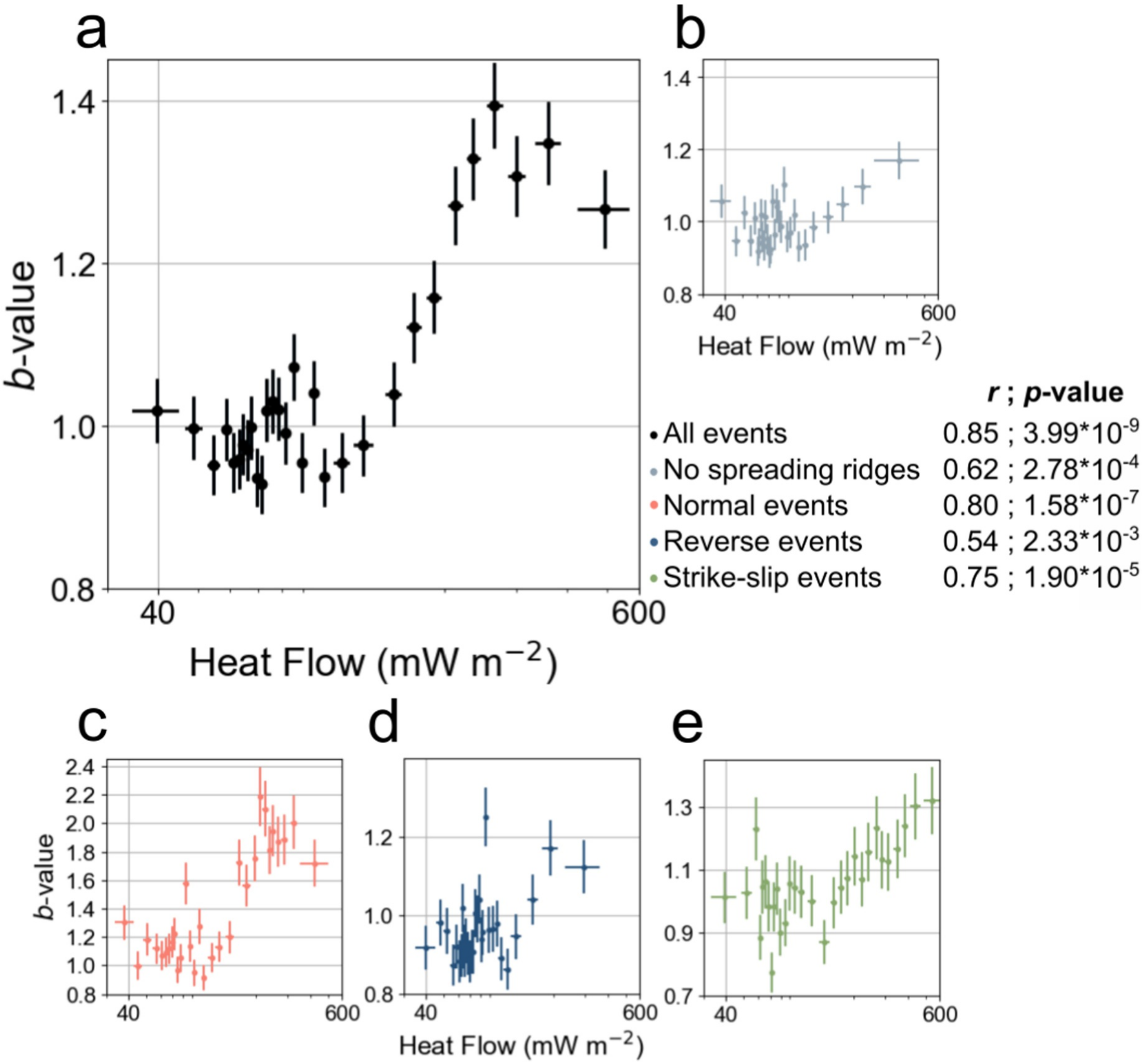

Figure 2. Correlation between b-value and heat flow. (a) Considering all the events in the catalog above the completeness magnitude (M_C); (b) Excluding events that occurred in spreading ridges. For confirmatory results obtained using a more conservative estimation of the M_C and a different number of intervals, see Figure S2 in Supporting Information S1; (c–e) Considering all the events and grouping them according to the focal mechanism (red for normal events, blue for reverse events and green for strike slip events). Horizontal error bars represent the standard deviation of the heat flow, while the vertical bars indicate the uncertainty on the estimation of the b-value (Equation 2). For confirmatory results obtained using the second solution of the CMT, a more conservative estimation of the M_C and a different number of intervals see Figure S3 in Supporting Information S1 and using a more conservative estimation of the M_C and a different number of intervals, see Figure S4 in Supporting Information S1.

environments (Bird & Kagan, 2004; Kagan et al., 2010). In spreading ridges, the heat flow is particularly high, but ridges are also characterized by a relatively young and thin crust, which may limit the maximum magnitude and impact the b-value (Bird & Kagan, 2004; Laske et al., 2013). To overcome this circular argument and to investigate if the heat flow is the main driver, independently from these peculiar conditions of spreading ridges, we repeat the same analysis in two other conditions: (a) by excluding all the events occurring along spreading ridges (Bird, 2003), and (b) by adopting a tapered Gutenberg-Richter distribution to minimize the impact of potential shortages in large magnitudes due to a thin crust. In both cases, the trend remains similar, excluding the possibility that the correlation is only driven by events in spreading ridges (Figure 2b) or by a potential shortage of large events. This finding suggests that variations in heat flow may influence the variation of b-values consistently across different tectonic settings.

10.1029/2025GL120494

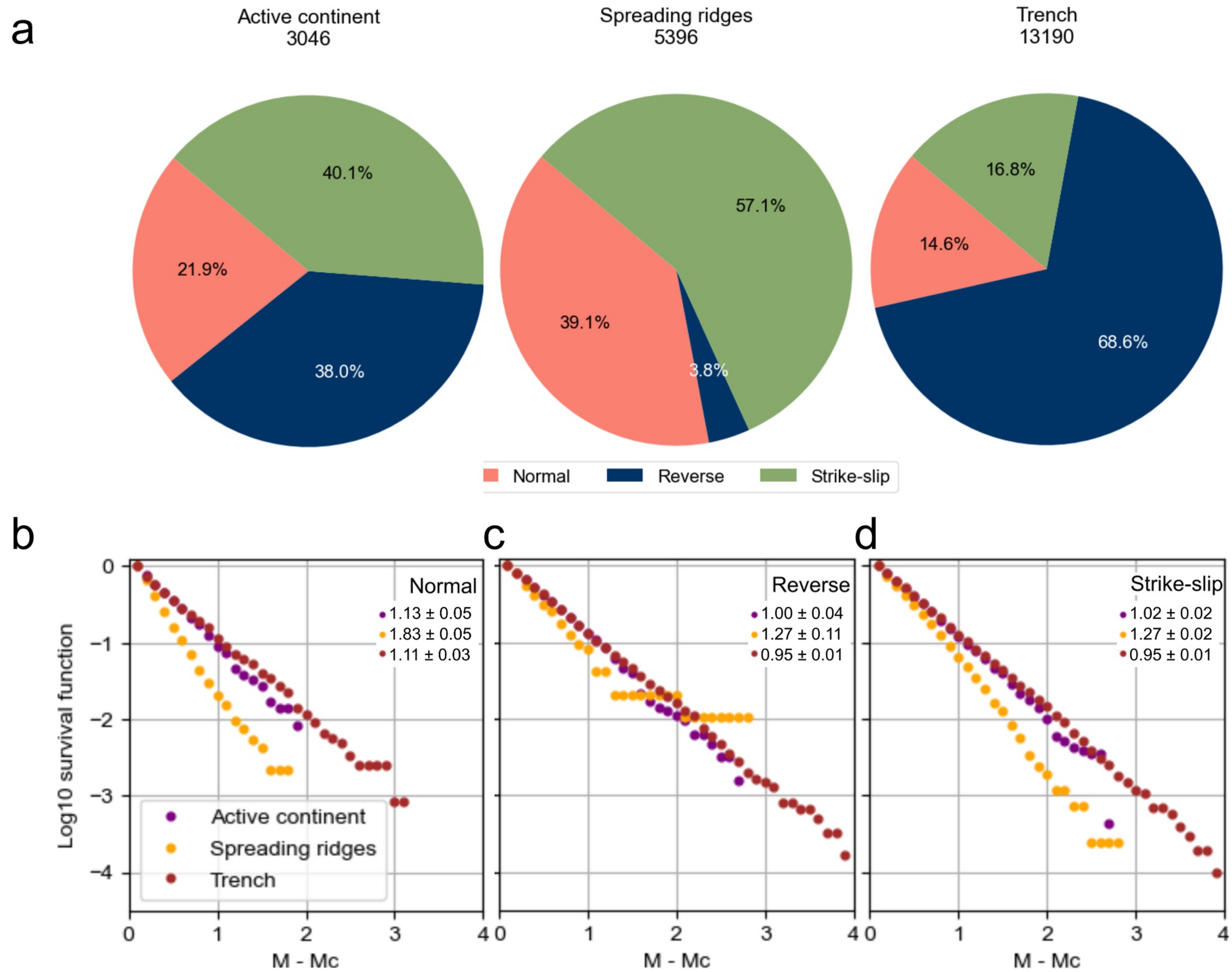

Figure 3. Distribution of focal mechanisms in each tectonic environment and their magnitude-frequency distributions. Panel (a) Percentages of occurrence of normal (blue), reverse (green), and strike-slip (red) events in each tectonic environment. The total number of events in each environment is at the top of each chart. For confirmatory results based on the second solution of the CMT and using a more conservative completeness magnitude (M_C), see Figure S7 in Supporting Information S1. Panel (b) magnitude-frequency distributions for each focal mechanism grouping according to the tectonic environment (Bird, 2003). The *b*-values are listed in the top-right corner. For confirmatory results based on the second solution of the CMT and using a more conservative M_C, see Figure S8 in Supporting Information S1.

To strengthen our analysis, we divide the magnitudes into two groups based on mean heat flow: one for values below 132 mWm^{-2} and one for values above this threshold (Figure S6 in Supporting Information S1). We then employ two statistical tests (see Section 2 and Figure S6 legends in Supporting Information S1) to compare the MFDs and the *b*-values between the two groups, finding that MFDs and *b*-values are significantly different. Still, even when excluding events from spreading ridges, the two distributions remain consistently different.

The observed trends also explain the *b*-value variations as a function of the focal mechanism. This variation is usually interpreted as the effect of the stress that changes systematically between different faulting regimes (Petruccelli et al., 2019; Schorlemmer et al., 2005). However, faulting styles are not uniformly distributed in the different tectonic environments (Figure 3a), which are characterized by different *b*-values (Figure 3b) and by different heat flows (Figure S5 and Table S3 in Supporting Information S1), with higher *b*-values in spreading ridges where normal faults are prevalent relative to other tectonic environments. As above, to overcome this circular argument and to investigate if the heat flow is the main driver, we repeat the analysis by grouping the events for focal mechanisms, using the three main faulting styles: normal, reverse, and strike-slip. We find that the significant trend between *b*-value and heat flow still holds for all the main faulting mechanisms (Figures 2c–2e), showing that dependence applies to all individual focal mechanisms and goes beyond any direct dependence between the focal mechanism and *b*-value.

To assess whether our data also exhibit the type of nonlinear behavior described in previous studies, we perform a dedicated evaluation of the heat flow-*b*-value relationship. In particular, we test three alternative thresholds to partition the data set: the 84 mWm^{-2} value proposed by Cheng et al. (2020), the mean heat flow value for each subset, and the heat flow value corresponding to the minimum *b*-value observed in our curves (Table S4 in Supporting Information S1). For each threshold, we independently examine the correlation below and above the partition. Across all tests, the results are consistent: a significant positive correlation is always identified above the threshold, whereas no significant correlation is ever detected below it. Although a shallow minimum *b*-value curve may be visually apparent, our statistical analyses indicate that this feature is not significant.

These results are partially consistent with the findings of Cheng et al. (2020), who identify a nonlinear relationship between heat flow and earthquake magnitude distribution, characterized by a decrease in the *b*-value for heat flow values below 84 mWm^{-2} and an increase above this threshold. While our data exhibit a visually similar pattern, statistical testing (Table S4 in Supporting Information S1) indicates that the apparent decrease at low heat flow is not significant, whereas the positive correlation observed at higher heat flow values is robust. This difference likely reflects both the broader tectonic coverage and the more homogeneous magnitude and mechanism estimates provided by the GCMT catalog, as well out explicit treatment of temporal variations in completeness.

Our findings are consistent with recent advances in understanding earthquake clustering style and its dependence on crustal properties. Using the nearest-neighbor approach, Zaliapin and Ben-Zion (2013a, 2013b) identify two main types of seismic clusters: burst-like sequences, characterized by rapid brittle failure and a dominant mainshock, and swarm-like sequences, reflecting mixed brittle–ductile behavior with distributed energy release. These cluster types show distinct geographic distributions controlled by heat flow and crustal viscosity: burst-like clusters prevail in cold, dry regions, whereas swarm-like clusters dominate in hot, fluid-rich areas. These patterns are subsequently confirmed at the global scale by Zaliapin and Ben-Zion (2016) and demonstrate that heat flow exerts primary control over clustering style across diverse tectonic environments. In agreement with our results, their analysis demonstrates that the heat flow is the dominant controlling factor, with the type and intensity of lithospheric deformation (measured by strain rate tensor parameters) playing a secondary role in determining earthquake cluster style.

This framework explains both clustering behavior and *b*-value variability in our study. In cold regions with low heat flow and low fluid content, higher effective viscosity promotes brittle rupture, strong stress heterogeneity, and lower triggering potential—resulting in burst-like clustering and lower *b*-values. Conversely, in hot regions with abundant fluids and low viscosity, mixed brittle–ductile deformation enhances triggering and swarm-like clustering, producing higher *b*-values.

Although our results show that heat flow represents the first-order control, we argue that the *b*-value could be also influenced by a set of competing conditions, such as fault distribution, stress state, lithology, crustal damage, and fluid content.

5. Conclusions

Our results highlight the complexity of physical factors influencing the earthquake MFD. The global analysis, including diverse crustal conditions, reveals that heat flow is the main control of the *b*-value variations, consistently across different tectonic regimes and faulting styles. High *b*-values are systematically associated with high heat flow, regardless of the tectonic environment and faulting style. This suggests that thermal conditions are a powerful tool for discriminating zones with higher seismogenic potential, surpassing tectonics and kinematics. Notably, we also demonstrate that the trend is not governed only by the thickness of the crust or by the lack of large events.

At first order, regions with high heat flow exhibit higher *b*-values, reflecting the thermally controlled nature of their seismogenic process. Consequently, these regions also tend to experience fewer very large earthquakes, consistent with global observations from the past 120 years (Pacheco & Sykes, 1992; Ekström et al., 2012, Figure S9 in Supporting Information S1) and explains the relatively low frequency of large events in spreading ridges and certain subduction zones (Kagan et al., 2010; Marzocchi et al., 2016; Taroni et al., 2021). The systematic variation in maximum observed magnitude—from cold, contracting subduction zones to hot, spreading ridges—directly reflects the thermal control on the upper bound of the magnitude distribution.

Overall, this study provides new insights into the drivers of *b*-value variability, emphasizing the importance of thermal conditions in their interpretation. By demonstrating the *b*-value reflects the interplay of multiple physical factors-with heat flow acting as the dominant but not exclusive control-offers a unified framework for interpreting regional differences in seismicity. This approach could enhance the interpretation of *b*-value variations and improve hazard forecasts and risk mitigation strategies in seismically active regions.

Conflict of Interest

The authors declare no conflicts of interest relevant to this study.

Data Availability Statement

The earthquake catalog used in the study is available at Global CMT Catalog Search via https://www.globalcmt.org/CMTsearch.html.

Version 1.15.3 of SciPy used to calculate the Pearson correlation coefficient and corresponding *p*-value and the *p*-value of the two-sample Kolmogorov-Smirnov test is preserved at https://doi.org/10.1038/s41592-019-0686-2, https://scipy.org (Virtanen et al., 2020, last accessed January 2025).

We also used the implementation of Taroni (2023) to calculate the completeness magnitude. We used the implementation of Taroni (2021) and Taroni et al. (2021) to calculate the *b*-value.

The data set and software are accessible at Corrado et al. (2025). *b*-value versus heat flow data set and code Zenodo. https://doi.org/10.5281/zenodo.15727476.

Acknowledgments

This study was supported by the Istituto Nazionale di Geofisica e Vulcanologia (INGV) in task “Analisi Statistiche” of macroarea “Monitoraggio Sismico, Geodetico, Acustico” of the projects “Reti Multiparametriche” and “Progetto Centro Italia (DL50)”. We received further support from the “Testing the potential impact of foreshock occurrence in the improvement of seismic risk managment” project, funded by the European Union's NextGenerationEU and the Italian Ministry of University and Research (MUR) under the “Fondo per il Programma Nazionale di Ricerca e Progetti di Rilevante Interesse Nazionale” (PRIN; Code P202247YKL). M. T. was supported by the INGV within the framework of the SECURE project - part of Pianeta Dinamico (Working Earth) - Geosciences for the Understanding of the Dynamics of the Earth and the Consequent Natural Risks (CUP code D53J19000170001), funded by the Italian Ministry of University and Research (MIUR). Open access publishing facilitated by Universita degli Studi di Napoli Federico II, as part of the Wiley - CRUI-CARE agreement.

References

Aki, K. (1965). A note on the use of microseisms in determining the shallow structures of the earth’s crust. *Geophysics*, *30*(4), 665–666. https://doi.org/10.1190/1.1439640

Aki, K. (1981). A probabilistic synthesis of precursory phenomena. *Earthquake prediction: an international review*, *4*, 566–574. https://doi.org/10.1029/ME004p0566

Aki, K., & Richards, P. G. (2002). *Quantitative seismology*. University Science Books.

Amitrano, D. (2003). Brittle-ductile transition and associated seismicity: Experimental and numerical studies and relationship with the b value. *Journal of Geophysical Research*, *108*(B1), 2044. https://doi.org/10.1029/2001JB000680

Anderson, E. M. (1905). The dynamics of faulting. *Transactions of the Edinburgh Geological Society*, *8*(3), 387–402. https://doi.org/10.1144/transed.8.3.387

Bird, P. (2003). An updated digital model of plate boundaries. *Geochemistry, Geophysics, Geosystems*, *4*(3), 1027. https://doi.org/10.1029/2001GC000252

Bird, P., & Kagan, Y. Y. (2004). Plate-tectonic analysis of shallow seismicity: Apparent boundary width, beta, corner magnitude, coupled lithosphere thickness, and coupling in seven tectonic settings. *Bulletin of the Seismological Society of America*, *94*(6), 2380–2399. https://doi.org/10.1785/0120030107

Bonferroni, C. (1936). *Teoria statistica delle classi e calcolo delle probabilita* (Vol. 8, pp. 3–62). Pubblicazioni del R istituto superiore di scienze economiche e commerciali di firenze.

Cheng, C., Hui, C., Yang, J., & Shen, S. (2020). The relationship between heat flow and seismicity in global tectonically active zones. *Open Geosciences*, *12*(1), 1430–1439. https://doi.org/10.1515/geo-2020-0195

Collettini, C., & Tinti, E. (2025). The influence of lithology and fault source volume on the magnitude–frequency-distribution of earthquakes. *Geophysical Research*, *52*, 2. https://doi.org/10.1029/2024GL110354

Corrado, P., Herrmann, M., & Marzocchi, W. (2025). Earthquake magnitude correlations expose short-term catalog incompleteness. *Seismological Research Letters*, *96*(2A), 909–919. https://doi.org/10.1785/0220240277

Davies, J. H. (2013). Global map of solid Earth surface heat flow. *Geochemistry, Geophysics, Geosystems*, *14*(10), 4608–4622. https://doi.org/10.1002/ggge.20271

Dziewonski, A. M., Chou, T. A., & Woodhouse, J. H. (1981). Determination of earthquake source parameters from waveform data for studies of global and regional seismicity. *Journal of Geophysical Research*, *86*(B4), 2825–2852. https://doi.org/10.1029/JB086iB04p02825

Ekström, G., Nettles, M., & Dziewonski, A. M. (2012). The global CMT project 2004-2010: Centroid-moment tensors for 13,017 earthquakes. *Physics of the Earth and Planetary Interiors*, *200–201*, 1–9. https://doi.org/10.1016/j.pepi.2012.04.002

Enescu, B., Hainzl, S., & Ben-Zion, Y. (2009). Correlations of seismicity patterns in Southern California with surface heat flow data. *Bulletin of the Seismological Society of America*, *99*(6), 3114–3123. https://doi.org/10.1785/0120080038

Gibbons, J. D., & Chakraborti, S. (2003). Nonparametric statistical inference fourth edition, revised and expanded (statistics textbooks and monographs). https://doi.org/10.4324/9780203911563

Goebel, W. T. H., Schorlemmer, D., Becker, T. W., Dresen, G., & Sammis, C. G. (2013). Acoustic emissions document stress changes over many seismic cycles in stick-slip experiments. *Geophys. Res*, *40*(10), 2049–2054. https://doi.org/10.1002/grl.50507

González, Á. (2024). Improvements and heterogeneities of the Global Centroid Moment tensor catalog. *Seismological Research Letters*, *95*(6), 3566–3578. https://doi.org/10.1785/0220240272

Gulia, L., Rinaldi, A. P., Tormann, T., Vannucci, G., Enescu, B., & Wiemer, S. (2018). The effect of a mainshock on the size distribution of the aftershocks. *Geophys. Res*, *45*(24), 13277–13287. https://doi.org/10.1029/2018GL080619

Gulia, L., & Wiemer, S. (2010). The influence of tectonic regimes on the earthquake size distribution: A case study for Italy. *Geophysical Research*, *37*(10), L10305. https://doi.org/10.1029/2010GL043066

Gulia, L., Wiemer, S., & Vannucci, G. (2020). Pseudoprospective evaluation of the foreshock traffic-light system in ridgecrest and implications for aftershock hazard assessment. *Seismological Research Letters*, *91*(5), 2828–2842. https://doi.org/10.1785/0220190307

Herrmann, M., & Marzocchi, W. (2021). Inconsistencies and lurking pitfalls in the magnitude–frequency distribution of high-resolution earthquake catalogs. *Seismological Research Letters*, *92*(2A), 909–922. https://doi.org/10.1785/0220200337

Hirata, T. (1989). A correlation between the b value and the fractal dimension of earthquakes. *Journal of Geophysical Research*, *94*(B6), 7507–7514. https://doi.org/10.1029/JB094iB06p07507

Iwata, T. (2008). Low detection capability of global earthquakes after the occurrence of large earthquakes: Investigation of the Harvard CMT catalogue. *Geophysical Journal International*, *174*(3), 849–856. https://doi.org/10.1111/j.1365-246X.2008.03864.x

Kagan, Y. Y. (1999). "Is Earthquake Seismology a Hard, Quantitative Science?" in seismicity patterns, their statistical significance and physical meaning. In *Pageoph topical volumes* (pp. 233–258). Birkhäuser. https://doi.org/10.1007/978-3-0348-8677-2_3

Kagan, Y. Y. (2002). Seismic moment distribution revisited: I. Statistical results. *Geophysical Journal International*, *148*(3), 520–541. https://doi.org/10.1046/j.1365-246x.2002.01594.x

Kagan, Y. Y. (2003). Accuracy of modern global earthquake catalogs. *Physics of the Earth and Planetary Interiors*, *135*(2–3), 173–209. https://doi.org/10.1016/S0031-9201(02)00214-5

Kagan, Y. Y. (2004). Short-term properties of earthquake catalogs and models of earthquake source. *Bulletin of the Seismological Society of America*, *94*(4), 1207–1228.

Kagan, Y. Y., Bird, P., & Jackson, D. D. (2010). Earthquake patterns in diverse tectonic zones of the globe. *Pure and Applied Geophysics*, *167*(6–7), 721–741. https://doi.org/10.1007/s00024-010-0075-3

Laske, G., Masters, G., Ma, Z., & Pasyanos, M. (2013). Update on CRUST1.0—A 1-degree global model of Earth's crust. In *Geophysical research abstracts* (Vol. 15, p. 2658).

Lippiello, E., & Petrillo, G. (2024). *b*-more-incomplete and *b*-more-positive: Insights on a robust estimator of magnitude distribution. *Journal of Geophysical Research: Solid Earth*, *129*(2), e2023JB027849.

Manganiello, E., Herrmann, M., & Marzocchi, W. (2023). New physical implications from revisiting foreshock activity in southern California. *Geophysical Research*, *50*(1), e2022GL098737. https://doi.org/10.1029/2022GL098737

Marzocchi, W., Sandri, L., Heuret, A., & Funiciello, F. (2016). Where giant earthquakes may come. *Journal of Geophysical Research: Solid Earth*, *121*(10), 7322–7336. https://doi.org/10.1002/2016JB013054

Marzocchi, W., Spassiani, I., Stallone, A., & Taroni, M. (2020). How to be fooled searching for significant variations of the b-value. *Geophysical Journal International*, *220*(3), 1845–1865. https://doi.org/10.1093/gji/ggz541

Nandan, S., Ouillon, G., Wiemer, S., & Sornette, D. (2017). Objective estimation of spatially variable parameters of epidemic type aftershock sequence model: Application to California. *Journal of Geophysical Research: Solid Earth*, *122*(7), 5118–5143. https://doi.org/10.1002/2016JB013266

Pacheco, J. F., & Sykes, L. R. (1992). Seismic moment catalog of large shallow earthquakes, 1900 to 1989. *Bulletin of the Seismological Society of America*, *82*(3), 1306–1349. https://doi.org/10.1785/BSSA0820031306

Petruccelli, A., Schorlemmer, D., Tormann, T., Rinaldi, A. P., Wiemer, S., Gasperini, P., & Vannucci, G. (2019). The influence of faulting style on the size-distribution of global earthquakes. *Earth and Planetary Science Letters*, *527*, 115791. https://doi.org/10.1016/j.epsl.2019.115791

Petruccelli, A., Vannucci, G., Lolli, B., & Gasperini, P. (2018). Harmonic fluctuation of the slope of the frequency–magnitude distribution (b-value) as a function of the angle of rake. *Bulletin of the Seismological Society of America*, *108*(4), 1864–1876. https://doi.org/10.1785/0120170328

Scholz, C. H. (2015). On the stress dependence of the earthquake b value. *Geophysical Research Letters*, *42*(5), 1399–1402. https://doi.org/10.1002/2014GL062863

Schorlemmer, D., Wiemer, S., & Wyss, S. M. (2005). Variations in earthquake-size distribution across different stress regimes. *Nature*, *437*(7058), 539–542. https://doi.org/10.1038/nature04094

Taroni, M. (2021). Back to the future: Old methods for new estimation and test of the Gutenberg–Richter b-value for catalogues with variable completeness. *Geophysical Journal International*, *224*(1), 337–339. https://doi.org/10.1093/gji/ggaa464

Taroni, M. (2023). Estimating the magnitude of completeness of earthquake catalogs using a simple random variable transformation. *The Seismic Record*, *3*(3), 194–199. https://doi.org/10.1785/0320230017

Taroni, M., Selva, J., & Zhuang, J. (2021). Estimation of the tapered Gutenberg-Richter distribution parameters for catalogs with variable completeness: An application to the Atlantic ridge seismicity. *Applied Sciences*, *11*(24), 12166. https://doi.org/10.3390/app112412166

Tormann, T., Enescu, B., Woessner, J., & Wiemer, S. (2015). Randomness of megathrust earthquakes implied by rapid stress recovery after the Japan earthquake. *Nature Geoscience*, *8*(2), 152–158. https://doi.org/10.1038/ngeo2343

Utsu, T. (1966). A statistical significance test of the difference in b-value between two earthquake groups. *Journal of Physics of the Earth*, *14*(2), 37–40. https://doi.org/10.4294/jpe1952.14.37

van der Elst, N. J. (2021). B-positive: A robust estimator of aftershock magnitude distribution in transiently incomplete catalogs. *Journal of Geophysical Research: Solid Earth*, *126*(2). https://doi.org/10.1029/2020JB021027

Virtanen, P., Gommers, R., Oliphant, T. E., Haberland, M., Reddy, T., Cournapeau, D., et al. (2020). SciPy 1.0: Fundamental algorithms for scientific computing in Python. *Nature Methods*, *17*(3), 261–272. https://doi.org/10.1038/s41592-019-0686-2

Zaliapin, I., & Ben-Zion, Y. (2013a). Earthquake clusters in southern California I: Identification and stability. *Journal of Geophysical Research: Solid Earth*, *118*(6), 2847–2864. https://doi.org/10.1002/jgrb.50179

Zaliapin, I., & Ben-Zion, Y. (2013b). Earthquake clusters in southern California II: Classification and relation to physical properties of the crust. *Journal of Geophysical Research: Solid Earth*, *118*(6), 2865–2877. https://doi.org/10.1002/jgrb.50178

Zaliapin, I., & Ben-Zion, Y. (2016). A global classification and characterization of earthquake clusters. *Geophysical Journal International*, *207*(1), 608–634. https://doi.org/10.1093/gji/ggw300